

OPEN ACCESS

Review—Concentration Measurements In Molten Chloride Salts Using Electrochemical Methods

To cite this article: Tyler Williams *et al* 2021 *J. Electrochem. Soc.* **168** 123510

View the [article online](#) for updates and enhancements.

elementsix
DE BEERS GROUP



Element Six's boron doped diamond (BDD) is the ultimate material for electrochemical advanced oxidation processes

Free-standing BDD is the ideal electrode material for electrochemical applications as it possesses an extended solvent window and low capacitive current. It's also chemically and catalytically inert as well as extremely resistant to corrosion. BDD has no substrate and can withstand pH 1 - 14 operation.

Find out more and contact the team at ustechnologies@e6.com



e6.com/en/products/diamond-water-solutions



Review—Concentration Measurements In Molten Chloride Salts Using Electrochemical Methods

Tyler Williams,^z  Rankin Shum, and Devin Rappleye 

Department of Chemical Engineering, Brigham Young University, United States of America

The electrochemical measurement of concentration in molten chloride salts is a valuable tool for the control of existing and potential industrial processes, recycling of precious materials and energy production. The electrochemical techniques commonly used to measure concentration and each techniques' associated theory are discussed. Practices which improve measurement accuracy and precision are set forth. Exceptionally accurate and precise measurements published in the literature are evaluated based on their performance in specified concentration ranges. The strengths and weaknesses of the most accurate measurements are briefly explored. Chronopotentiometry (CP) and square wave voltammetry (SWV) are accurate and precise with low concentration measurements. SWV was accurate at low concentrations, even in multi-analyte mixtures. CP was accurate for only single analyte mixtures. Open-circuit potentiometry (OCP) is accurate and precise in single-analyte mixtures but yields large errors in multianalyte mixtures. Cyclic voltammetry (CV), chronoamperometry (CA) and normal pulse voltammetry (NPV) are accurate and precise across all concentration ranges. NPV is exceptionally well suited for measurements in melts with multiple electroactive species.

© 2021 The Author(s). Published on behalf of The Electrochemical Society by IOP Publishing Limited. This is an open access article distributed under the terms of the Creative Commons Attribution 4.0 License (CC BY, <http://creativecommons.org/licenses/by/4.0/>), which permits unrestricted reuse of the work in any medium, provided the original work is properly cited. [DOI: 10.1149/1945-7111/ac436a]



Manuscript submitted September 16, 2021; revised manuscript received November 5, 2021. Published December 24, 2021.

Molten chloride salts play a key role in producing critical materials and in innovative processes to mitigate carbon emissions and climate change impacts. They have found application in metal production, energy storage and production, nuclear material processing, and carbon capture and utilization. Magnesium and lithium metal is electrolytically produced at a commercial-scale from MgCl_2 melts and LiCl-KCl eutectic melts, respectively.^{1–6} Some rare earth metals have been commercially produced via electrolysis in fused chloride salts for several decades.⁷ More recent investigations have explored electrolytic reduction of rare earth oxides to metals or intermetallics.^{8,9} Substantial efforts have been devoted to developing the electrolytic oxide reduction of titanium and other metals in CaCl_2 .^{8–11} Molten chloride salts are being explored and developed for long-term thermal energy storage,^{12,13} concentrated solar power,^{14,15} and liquid metal batteries for grid-level energy storage.¹⁶ Nuclear reactors are being developed to utilize molten chloride salts as fuel and/or coolant.^{17–19} For decades, molten chloride salts, mainly CaCl_2 , NaCl-KCl and LiCl-KCl , have been used in pyrochemical processes to produce actinide metals.^{20–25} Recent research has demonstrated the ability to produce graphite from CO_2 in molten CaCl_2 .^{26,27} The ongoing commercial use and research in molten chloride salts demonstrate strong interest in further optimization and development of these processes.

The measurement of the composition within molten chloride salt processes in or near real time provides valuable insights into important behaviors and properties such as corrosion, electrodeposition, viscosity, density and melting points. Impurities have a significant impact on the corrosion of structural materials.^{28,29} In electrowinning and electrorefining, the electrodeposition rate, equilibrium potential, and morphology of specific metals depend upon the concentration of their ions in the salt.^{30,31} The accumulation of impurities can also affect the physical properties of molten salts which could result in poor flow and unexpected freezing in process lines and vessels, if unmonitored. In molten salt nuclear reactors, the constant fissioning and transmutation of atoms accumulates impurities, necessitating the constant monitoring and control of species in the molten salt.^{32,33} Additionally, in nuclear energy and material processing applications, there is also a need to track nuclear material with a specified degree of certainty and timeliness, in order to detect and deter the diversion of nuclear material for non-peaceful purposes.³⁴ Therefore, methods that could provide real-time or

near-real-time concentration measurements inside the harsh molten salt environment will provide valuable feedback to limit corrosion, optimize process parameters, and safeguard nuclear materials.

Several methods have been applied to measuring concentrations in molten chloride salts. A broad review of the methods applied to molten salts and pyroprocessing for concentration measurements and material accounting has been published.³⁵ However, due to the broad nature of the review, cyclic voltammetry (CV) is the only electrochemical method discussed. Electrochemical techniques lend themselves readily to in situ, rapid measurements of concentrations in molten salts due to their robust and simple hardware. Only 2 or 3 metal electrodes need to be immersed into the harsh molten salt environment to perform measurements. The sensitive electrical instruments (e.g., potentiostat) can be placed external to the harsh environment and connected to the electrodes via electrical feedthroughs. The metal electrodes measure electrical responses in the molten salt due to applied potentials or currents. These electrical responses are related to the concentration of ions in the molten salts. Despite the relative simplicity of the hardware, complications are introduced in relating concentration to the electrical responses due to nonideal behavior (e.g., surface area growth, migration, radial diffusion, ohmic resistance) and/or the misapplication of electrochemical theoretical relations. The practical aspects of performing electrochemical measurements in molten salts have recently been reviewed,³⁶ but the nuances of the analysis and application of electroanalytical measurements were briefly discussed with limited theoretical considerations. The objective of this review is to provide an in-depth analysis of published electrochemical data and methods used to measure concentrations in molten chloride salts and discuss the important details in analyzing and applying electrochemical theory and measurements in molten chloride systems.

Electroanalytical Techniques

Electroanalytical techniques have been applied to aqueous solutions for over a century. Lubert and Kalcher provide a history of electroanalytical techniques and trace their genesis back to the early 1800s.³⁷ In comparison, electroanalytical techniques in molten salts have a much younger history. According to Laitinen's synopsis of the history of electroanalytical techniques in molten salts, significant work begins in molten chloride salts in the 1950s.³⁸ Laitinen attributes the delay in pursuing electroanalytical techniques in molten chloride to their experimental difficulty. The compatibility of materials with molten salt systems needed to be addressed to

^zE-mail: wtlyerb@byu.edu

identify possible containers and electrodes. Due to their hygroscopic nature, preparation and purification methods for chloride salts also needed to be developed to limit hydrolysis and chemical attack of containers and electrodes. Because of this experimental difficulty, this section strives to provide a brief overview of electroanalytical methods commonly used in the literature to measure concentration with a focus on aspects unique to molten chloride salt systems. References are provided for each method that more comprehensively cover the assumptions, derivations, and applications of each method.

Among the assumptions made when deriving a mathematical model, the electrochemical reversibility of reactions and the phases of redox species are of special interest. Electrochemical reversibility typically refers to whether the electron transfer at the electrode surface is rapid enough that the surface concentrations immediately adjust to thermodynamic equilibrium. In other words, whether or not the Nernst equation can describe the concentration near the electrode surface. The phases of redox species are typically denoted as “soluble-soluble” or “soluble-insoluble,” where the first term refers to the reactants and the second to products. For example, metal deposition onto a solid inert electrode (e.g., reducing La^{3+} ions to La metal on W cathode) would be considered soluble-insoluble. Models which are derived for soluble-soluble reactions must account for ions transferring to and from the electrode surface, while soluble-insoluble models only account for ions transferring to the electrode surface.

The typical electrochemical cell is composed of three electrodes: a working electrode (WE), reference electrode (RE) and counter electrode (CE). To control and observe the electrochemistry occurring around the WE, the difference in electrochemical potential is measured between the WE and RE, while current is passed and measured through the WE and CE. Simply stated, potential and current measurements are made at the WE. The RE provides a stable reference potential for the WE with a reference solution separated from the bulk solution (i.e., the solution containing the WE and CE) by a membrane, typically. Pseudo- and quasi-RE are frequently used in molten chloride salts due to limitations on compatible membrane materials. These REs are typically metal wires immersed in the bulk solution with stable potentials over the timescales of electrochemical measurements, but their reference potential is unknown and will shift with changes in bulk solutions. A more in-depth treatment of the circuitry, experimental configurations, and other considerations behind electrochemical cell design can be found elsewhere.^{36,39}

Chronoamperometry (CA).—CA was pioneered and developed by Frederick Cottrell in 1903.⁴⁰ As illustrated in Fig. 1, CA is a potential step method that typically generates the current response characterized by the Cottrell equation^{39,40} to relate the diffusion controlled or diffusional current (I_d) to concentration,

$$I_d(t) = nFAC_i^* \sqrt{\frac{D_i}{\pi t}} \quad [1]$$

Where n is number of electrons exchanged, F is Faraday’s constant, A is the area of the electrode, D_i is the diffusion coefficient of the analyte ion (i), t is elapsed time from the beginning of the potential step, and C_i^* is the bulk concentration of the analyte. The Cottrell equation is derived from Fick’s second law of diffusion with initial and boundary conditions of uniform bulk concentration of i at $t = 0$, constant bulk concentration of i far away from the electrode surface, and no i at the electrode surface.^{39–41} The basis of this derivation assumes that the analyte is dilute enough that migration is negligible, the diffusion coefficient is constant, and the current is diffusion controlled. The assumption of diffusion control can be verified by comparing the current response at varying potential step sizes. If sufficient time has elapsed between potential steps for the diffusion layer to fully relax (i.e., concentration gradients in diffusion layer have been eliminated), then the current at each potential step size will be identical when controlled by diffusion. The Cottrell equation

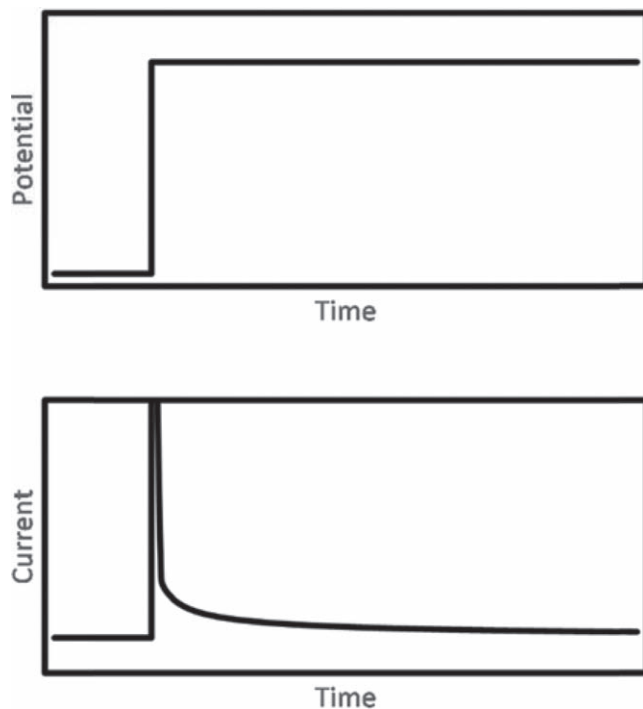


Figure 1. Illustrated waveform (top) and response (bottom) for CA.

can be applied to both soluble-soluble and soluble-insoluble systems because the derivation does not consider the electrochemical reaction products.

Sampling time range is an important parameter to optimize. Too short of sampling times may introduce significant measurement error due to double layer charging. In most molten salt electroanalytical cells, the double-layer charging current is negligible after 0.01 seconds, but this depends on the material, spacing and surface area of the electrodes, the resistance of the molten salt (R_s), and capacitance of the double layer (C_d). To ensure that unwanted artifacts from double-layer charging are not included, the time constant ($R_s C_d$) should be determined for the specific experimental setup and sampling times less than $3R_s C_d$ should be avoided or excluded when using 1. Too long of sampling times may result in radial diffusion effects, if using a cylindrical wire or rod for the WE. The CA response of a cylindrical electrode differs from 1 by more than 4% when,^{39,42}

$$\frac{4D_i t}{r^2} > 0.01. \quad [2]$$

For a cylindrical electrode with a 0.5 mm radius (r), that would correspond to 1.25 s, assuming a diffusion coefficient of $10^{-5} \text{ cm}^2 \text{ s}^{-1}$. In the case of metal deposition, WE area growth at long times and nucleation effects at short times can cause deviations from the behavior predicted by 1.⁴³

Cyclic voltammetry.—The associated waveform and a typical response for a soluble-insoluble reaction is found in Fig. 2. CV scans the WE potential between an upper and lower limit at a specified scan rate (ν). The scan reverses direction at a switching potential (E_s). When a WE potential is reached at which an analyte in the solution is reduced or oxidized, the current rises, forms a peak (I_p) and decays.

There are many well defined relations associated with CV. These relations predict E vs I curves, peak height, peak width, peak width at half height and peak separation. CVs can discern reactions, reaction steps, the reversibility of the reaction, and the solubility of products. However, analysis is often complicated by non-idealities,

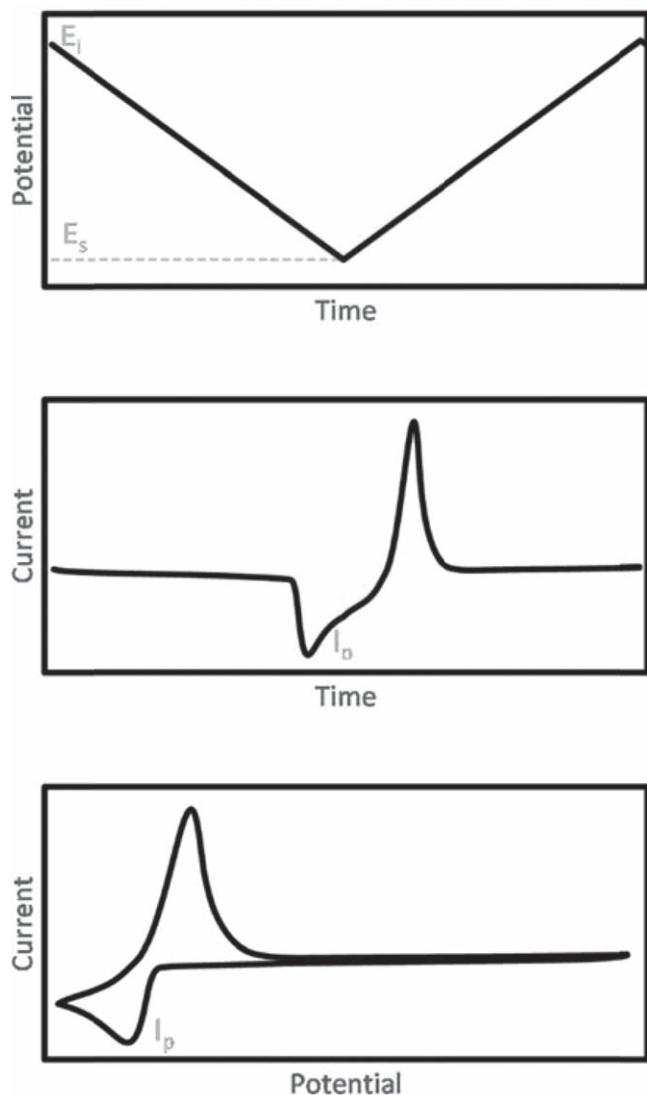


Figure 2. Illustrated waveform (top) and response (middle and bottom) for CV.

such as overlapping peaks, resistance effects, and surface area growth. Additionally, the selection of an appropriate quantitative relation is dependent upon the phases of redox species and the electrochemical reversibility of reaction. Some common mathematical relations intended for analyzing CVs are found in Table I. Each relation has the common assumptions of no migration nor convection, semi-infinite linear diffusion, at $t = 0$ only the oxidized species is present, C_O^* is constant and $C_R^* = 0$. Relations for soluble-soluble reversible reactions were developed by John Randles and A. Ševčík in 1948.^{44,45} The soluble-insoluble relations for reversible reactions were developed by Talivaldis Berzins and Paul Delahay in 1953.⁴⁶ Paul Delahay also produced the irreversible theory in that same year.⁴⁷ Hiroaki Matsuda and Yuzo Ayabe developed the relations and dimensionless parameters for soluble-soluble quasi-reversible reactions in 1955.⁴⁸ Not included in the Table I, but of note, Atek et al. have derived and validated semi-analytical solutions for linear sweep voltammetry (LSV) of quasi-reversible, soluble-insoluble reactions using the same assumptions as the relations in Table I and the additional assumptions of instantaneous nucleation and complete metal coverage on the WE (i.e., activity of metal deposit is one).⁴⁹ Dimensionless parameters have been developed to delineate between the reversible, quasi-reversible and irreversible regimes for soluble-soluble and soluble-insoluble CVs and are given in Table II.

Variables, such as scan rate, can influence the reversibility of the system. It is good practice to verify a system's compliance with the associated assumptions of a model before use. This is commonly done by plotting the peak current vs the square root of scan rate and peak potential vs the logarithm (or natural log) of scan rate. As shown in the relations in Table I, if the peak current is linear with square root of scan rate and the peak potential is independent of scan rate, then reversibility is presumed to be verified. This is often sufficient, but not always. Shen and Alkolkar's initial analysis of Nd deposition revealed a linear proportionality between cathodic peak current density and square root of scan rate. By comparing values computed from the models with the data taken, it was found that the data did not follow the Berzins-Delahay model. The subsequent development of an applicable model revealed that the reduction peak of Nd onto W is complicated by a multi-step reaction with an intermediate species.⁵¹

In the case of metal deposition, surface area growth may affect peak height at low scan rates or high concentrations. Because CV is a potential sweep method, the metal deposits continuously leading up to the peak. If sufficient charge is passed before the peak, enough metal may deposit before the peak to augment the WE area, making the current density uncertain.

Compensating for resistances when making potential sweep measurements is vital to generating a waveform with a consistent scan rate. When current begins to rise in a CV so does the potential required to overcome ohmic resistance ($E = IR$). If active compensation or waveform adjustments for the potential drop due to ohmic resistance are not employed, the peak current is artificially depressed because the CV waveform becomes distorted with slower scan rates near the peaks and faster scan rates away from the peaks.^{52–55} Although solution resistance in molten chloride salts is generally low ($<1 \Omega$), ohmic drop becomes significant at higher scan rates and concentrations. Hence, uncompensated resistance distorts the relationship between peak current and concentration introducing error.^{52,55}

Normal pulse voltammetry (NPV).—NPV builds upon CA by performing a series of potential measurements with a rest or interval time (t_i) in between each step, as illustrated in Fig. 3. The potential during the interval time is set at a value that will renew the electrode surface and diffusion layer. Each subsequent potential step is shifted by a step potential (ΔE_s). The current is sampled consistently for each potential step at the pulse time (t_p)—the end of the potential pulse. Eventually, the sampled current reaches a consistent value called the diffusional current (I_d) which is given by 1, but at t_p . Early instrumentation work for NPV was accomplished by G.C. Barker and A.W. Gardner in 1960.⁵⁶ One of the earliest applications of NPV to molten salt was accomplished by Osteryoung and Carlin in 1989.⁵⁷

$$I_d(t) = nFA \sqrt{\frac{D_i}{\pi t_p}} C_i^* \quad [16]$$

All the assumptions and considerations for 1 apply. Unique to NPV is the need to optimize the step potential, interval time, and rest potential to ensure adequate renewal of the electrode surface and diffusion layer. The diffusion layer can be 90% restored rapidly at a stationary electrode. Achieving renewals above 99% can require significant amount of time (≥ 15 s).^{58,59} Complete renewal of the diffusion layer may not be practical at a stationary, non-polarographic electrode, possibly requiring a ratio of interval to pulse time greater than 2500.⁵⁸ Rotating the electrode between pulses can provide more rapid renewal of the diffusion layer. The incomplete renewal becomes particularly problematic if the step potential is small, as observed by Zhang et al.⁶⁰ Smaller potential steps increase the number of steps with the incomplete renewal of the diffusion layer compounding with each additional step. For stationary electrodes, the step potential should be selected to achieve absolute

Table I. Standard mathematical models for CV.

Reversible (soluble-soluble)

Randles – Ševčík

$$I_p = 0.4463AC_0^* \sqrt{\frac{(nF)^3 D_O \nu}{RT}} \quad (3)$$

$$E_p = E^{0'} + \frac{RT}{nF} \ln \left(\sqrt{\frac{D_R}{D_O}} \right) - 1.109 \frac{RT}{nF} \quad (4)$$

$$\Delta E_p = |E_p - E_{p/2}| = 2.20 \frac{RT}{nF} \quad (5)$$

Quasi-Reversible (soluble-soluble)^{a)}

$$I_p = I_p(\text{rev})K(\Lambda, \alpha) \quad (9)$$

$$\Lambda = \frac{k^0}{\sqrt{D_O^{1-\alpha} D_R^{\alpha} \frac{nF\nu}{RT}}} \quad (10)$$

$$E_p = E^{0'} + \frac{RT}{nF} \ln \left(\sqrt{\frac{D_R}{D_O}} \right) - \Xi(\Lambda, \alpha) \frac{RT}{nF} \quad (11)$$

$$\Delta E_p = |E_p - E_{p/2}| = \Delta(\Lambda, \alpha) \frac{RT}{nF} \quad (12)$$

a) $K(\Lambda, \alpha)$, $\Xi(\Lambda, \alpha)$ and $\Delta(\Lambda, \alpha)$ are tabulated functions and may be found in Refs. 39, 48 b) $b = \frac{anF}{RT}$. ***Irreversible relations do not include reduced product in their derivation because anodic processes are assumed to be negligible.

Reversible (soluble-insoluble)

Berzins – Delahay

$$I_p = 0.6105AC_0^* \sqrt{\frac{(nF)^3 D_O \nu}{RT}} \quad (6)$$

$$E_p = E^{0'} + \frac{RT}{nF} \ln(x_O) - 0.854 \frac{RT}{nF} \quad (7)$$

$$\Delta E_p = |E_p - E_{p/2}| = 0.774 \frac{RT}{nF} \quad (8)$$

Irreversible (soluble)^{b)}*Delahay*

$$I_p = 0.4958AC_i^* \sqrt{\frac{\alpha(nF)^3 D_i \nu}{RT}} \quad (13)$$

$$E_p = E^{0'} + \frac{1}{b} \left(0.780 + \ln \left(\frac{\sqrt{D_O b \nu}}{k^0} \right) \right) \quad (14)$$

$$\Delta E_p = |E_p - E_{p/2}| = 1.857 \frac{RT}{anF} \quad (15)$$

Table II. Dimensionless parameters used to evaluate reversibility.

Reversibility	Soluble-Soluble ^{39,48}	Soluble-Insoluble ^{49,50}
Reversible	$\Lambda \geq 15$	$\omega \geq 10^{3a)}$
Quasi-Reversible	$15 \geq \Lambda \geq 10^{-2(1+\alpha)}$	$10^3 \geq \omega \geq 10^{-3}$
Irreversible	$\Lambda \leq 10^{-2(1+\alpha)}$	$\omega \leq 10^{-3}$

$$a) \Omega = k^0 (C_o^*/C_o)^\alpha \left(\pi D_o \frac{nF\nu}{RT} \right)^{-1/2}$$

minimum resolution needed to avoid accumulation or depletion of ions in the diffusion layer during NPV measurements.

Uncompensated resistance can affect the shape of the NPV curve by stretching it out. While *IR* compensation is not as essential in NPV or CA as in CV, uncompensated resistance can lead to an overestimation of concentration due to a shift in the *I* vs *t* decay curve. Once the overpotential is sufficient to overcome ohmic losses and achieve diffusion-controlled currents, the current will plateau. An important exception is at short times ($\ll 0.1$ s) and/or high resistances ($\gg 1 \Omega$) where deviations from Cottrellian behavior exist due to uncompensated resistance.^{59,61} For example, Åberg and Sharp calculated that Cottrellian behavior is not achieved until 0.01 s when the uncompensated resistance is 5 Ω .⁶¹

NPV is particularly advantageous for metal deposition because of the consistent renewal of the electrode surface and the diffusion layer. This minimizes surface area growth, which can limit the application of CV, and accumulation of ions in the diffusion layer after stripping. However, non-ideal effects, such as nucleation, need to be avoided or incorporated into the model.

Square wave voltammetry (SWV).—The initial technology and theory required for SWV was developed by many scientists. G.C. Barker and I.L. Jenkins developed the instrumentation for SWV and characterized the technique in 1952.⁶² Louis Ramaley and Matthew Krause made significant contributions to the reversible theory of SWV in 1969.⁶³ David Whelan, John O’Dea, Koichi Aoki, Janet Osteryoung, and Robert Osteryoung developed SWV theory for the study of kinetic systems, microelectrodes, and arbitrary electrode geometries in the 1980s.^{64–69}

SWV is a pulse method, like NPV. The waveform is defined by a step potential (ΔE_s), an amplitude (ΔE), and period ($2t_p$). A rectangular shaped wave is formed as shown in Fig. 4, where the step potential offsets the center of wave at the beginning of each period. The forward (I_f) and backward current (I_b) are recorded at

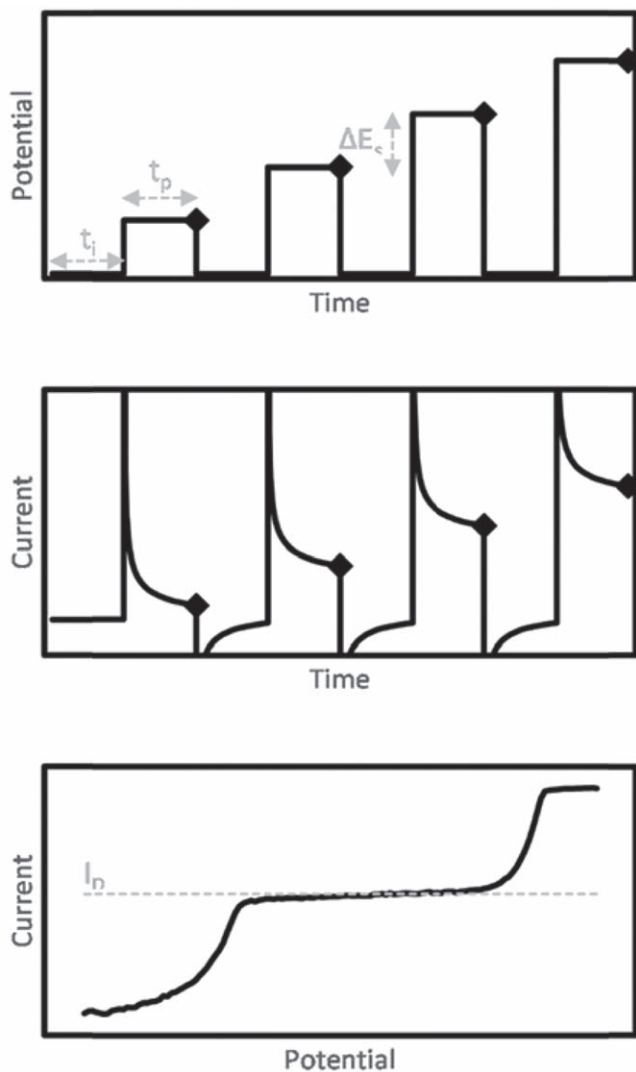


Figure 3. Illustrated waveform (top) and response (middle and bottom) for NPV. Diamonds represent that time at which the current is sampled.

the pulse time (t_p), indicated by the diamonds in Fig. 4. The

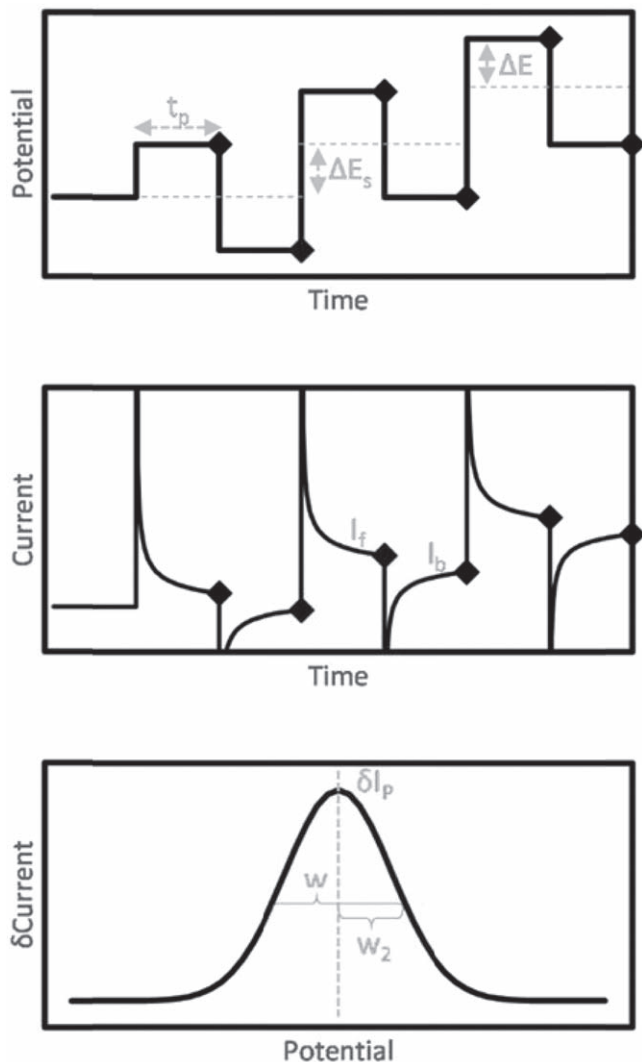


Figure 4. Illustrated waveform (top) and response (middle and bottom) for SWV.

difference between the forward and backward current within the same period yields the differential current (δI). The advantages of SWV are increased speed, background discrimination, and sensitivity. However, renewal of the WE surface and diffusion layer is not assured.

Features of the SWV commonly used in analysis are the differential peak current (δI_p), the full width at half maximum (w), and the back half of w (w_2). The back half of w is used primarily for metal deposition reactions to minimize the influence of nucleation effects. Electrochemical reversibility and product solubility can impact the value of these features. Furthermore, multiple parameters of SWV measurements influence the resulting features including pulse time, pulse amplitude, and step potential. Hence, careful parameter selection needs to be made when conducting SWV test to ensure the applicability of available models.

In a reversible, soluble-soluble system, w does not depend on pulse time, which is related to frequency (f),

$$f = \frac{1}{2t_p} \quad [17]$$

If $\frac{nF}{RT}\Delta E < 5$, the relation of w for a properly tuned SWV is given by⁷⁰

$$w = \frac{RT}{nF} \left[3.53 + \frac{3.46\xi^2}{\xi + 8.1} \right] \quad [18]$$

where $\xi = \frac{nF}{RT}\Delta E$, with minimal ($<0.047RT/nF$) error compared to the full expression derived by Aoki et al.⁷⁰ If $\xi < 0.5$, less than 3% error is introduced by further simplifying 18 to:^{71,72}

$$w = 3.53 \frac{RT}{nF} \quad [19]$$

The differential peak current is proportional to the square root of frequency or inversely related to the square root of pulse time, as shown in the equation below:^{39,71}

$$\delta I_p = nFA \sqrt{\frac{D_o}{\pi t_p}} C_o^* \Delta \psi_p(n, \Delta E_s, \Delta E) \quad [20]$$

where ψ is the dimensionless current created by normalizing by I_d . Values for $\Delta \psi_p$ have been tabulated, graphed, and presented elsewhere.^{39,71}

Fatouros and Krulic have developed SWV relations for reversible soluble-insoluble reactions under the assumption that a uniform monolayer is formed (i.e. two-dimensional nucleation), that absorption processes are reversible, and that surface area growth is significantly less than the diffusion layer thickness.⁷² The derived SWV expressions were validated for the $n = 1$ case. A simplified synopsis to their derived expressions is present here. To apply this simplified approach, the SWV parameters need to be:

$$0.04 \frac{RT}{nF} \leq |\Delta E_s| \leq 0.23 \frac{RT}{nF} \quad [21]$$

$$0.8 \frac{RT}{nF} \leq |\Delta E| \leq 4.7 \frac{RT}{nF} \quad [22]$$

$$t_p > \left(\frac{3.7\Gamma_1}{C_o^* \sqrt{D_o}} \right)^2 \quad [23]$$

where Γ_1 is monolayer density (i.e., moles per unit area) of the deposited metal. If condition 23 is met, then $\Delta \psi_p$ for metal deposition becomes independent of concentration and w_2 and δI_p are given by:

$$\delta I_p = nFA \sqrt{\frac{D_o}{\pi t_p}} C_o^* \Delta \psi_p(n, \Delta E_s, \Delta E) \quad [24]$$

$$w_2 = 0.7 \frac{RT}{nF} + 0.3nFAR_u C_o^* \sqrt{\frac{D_o}{t_p}} \quad [25]$$

It should be noted that the functional form of $\Delta \psi_p$ in 24 differs from the $\Delta \psi_p$ presented in 20. An approximate form of $\Delta \psi_p$ for metal deposition is presented by Fatouros and Krulic.⁷² The contribution of uncompensated resistance (R_u) to w_2 becomes less than 3% when:

$$t_p > \left(10 \frac{n^2 F^2 A R_u C_o^* \sqrt{D_o}}{RT} \right)^2 \quad [26]$$

and 25 can be simplified to:

$$w_2 = 0.7 \frac{RT}{nF} \quad [27]$$

The conditions in 21 and 26 diverge from each other as concentration changes making it difficult to satisfy both conditions at certain concentrations. In such cases, the more rigorous models for w_2 derived by Fatourus and Krulic may be required.

Studies have been published covering the quasi-reversible and irreversible behavior of SWV for soluble-soluble reactions.^{73–77} Similar to CV, the differential peak current decreases as the product of κ and t_p increases where:

$$\kappa = \frac{k^o}{D_o^{\alpha/2} D_R^{(1-\alpha)/2}} \quad [28]$$

Also, as κt_p increases, w is no longer constant. The change in w is dependent on α . At high values of κt_p , the differential peak potential becomes linear with $\log \sqrt{t_p}$. The behavior of differential peak current, potential, and width over the full range of κt_p from reversible to irreversible conditions have been presented elsewhere.^{73–75} To our knowledge, a theory for the behavior of quasi-reversible and irreversible soluble-insoluble reactions has not been derived.

Chronopotentiometry (CP).—CP, unlike the rest of the measurement techniques, is a galvanostatic method. As defined in this work, all CP is constant current. Current is applied at a constant value, while the potential shifts to maintain the electrochemical reaction rate. The associated waveform and response of CP is found in Fig. 5.

Because constant current also represents constant flux, the mathematics of CP is much simpler than other electrochemical techniques. However, difficulties in analysis are significant. The determination of transition time (τ), which is integral to the theory, is not well defined. Additionally, double-layer charging plays a significant role and even rudimentary corrections depend on τ .

The Sand equation,^{39,78} Eq. 29, was derived by Henry Sand in 1901 with the assumptions of semi-infinite linear diffusion, and no migration nor convection,

$$\frac{I\tau^{1/2}}{C_o^*} = \frac{nFAD_o^{1/2}\pi^{1/2}}{2} \quad [29]$$

where transition time (τ) may be approximated by drawing tangent lines at the inflection points found on either side of a plateau, drawing a tangent line for the plateau, and taking the difference in time of the intersections as τ . Another method for calculating τ is to measure from the departure of the curve from the tangent line of the inflection point prior to the plateau and the beginning of the curve's next plateau.⁷⁹ However, neither method has a strong theoretical basis. Rudimentary corrections for charging current (I_c) are available by the fitting of a line to $I\tau$ vs $\tau^{1/2}$, where the y-intercept is $I_c\tau$.³⁹

Open-circuit potentiometry (OCP).—In OCP, no significant current is allowed to flow through the circuit and the potential difference between the WE and RE is measured. A response typical of this method is displayed in Fig. 6.

OCP is a remarkably simple electrochemical technique because kinetics and mass transfer are not considered. However theoretically, the activity of all species in the system affects the potential, even those in the gaseous state. For instance, Smith et al. found that changing the composition of binary salts and ternary salts affected the partial vapor pressures and apparent activities of all species within the system.⁸⁰ Practical applications in industry where multiple species are likely to be present are problematic. Furthermore, the stability and consistency of the RE is critical in making OCP measurements.

The mathematical model used for OCP measurements is the Nernst equation which assumes equilibrium. Walther Nernst developed this equation in 1887,⁸¹ and Gilbert Lewis gave the more modern form when he proposed the concept of activity in 1907.⁸² Lewis' form has been depicted in 30, rather than the typical

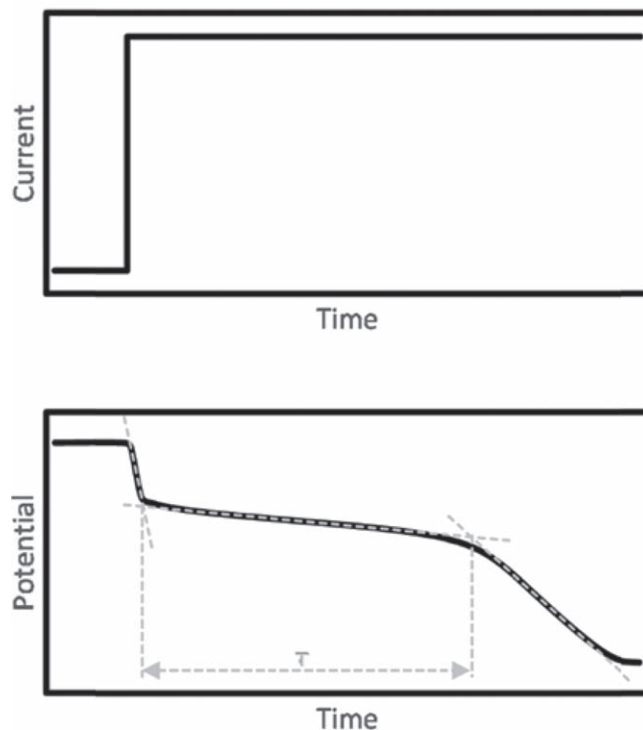


Figure 5. Illustrated waveform (top) and response (bottom) for CP.

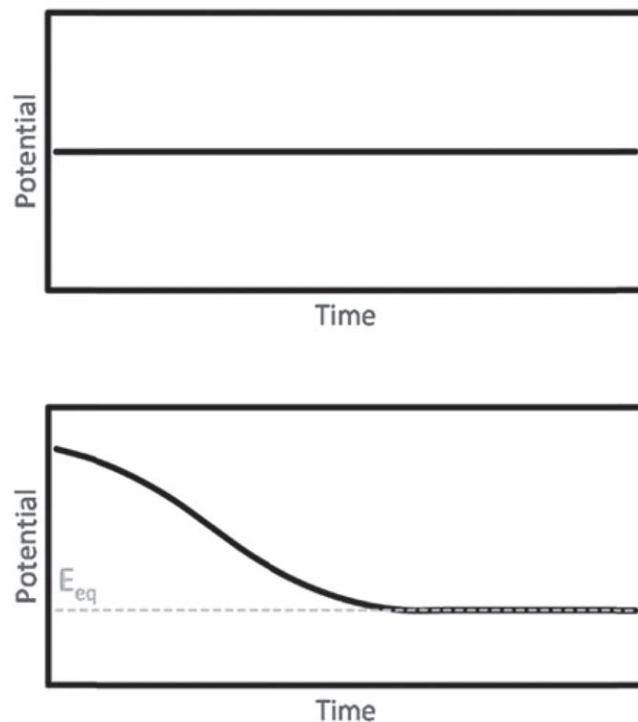


Figure 6. Illustrated waveform (top) and response (bottom) for OCP.

substitution of concentration for activity, because of the frequency of deposition reactions in molten salt electrochemistry.

$$E = E^0 + \frac{RT}{nF} \ln \frac{a_o^{\nu_o}}{a_R^{\nu_R}} \quad [30]$$

In 30, E is the measured potential, E^0 is the standard reduction potential, and ν_i is the appropriate stoichiometric coefficient.

Generally, the activities (a_i) are approximated as concentrations or mole fractions for soluble species and as 1 for solids composed of at least one monolayer. Because of the exponential relationship between potential and concentration (or activity), millivolt differences in the reference potential can introduce significant error. For instance, a system at 500 °C with a $n = 3$ reaction will predict concentrations with 4.6% and 25.3% relative error when E^0 is off by 1 mV and 5 mV, respectively. Similarly, activity coefficients can have a significant impact on OCP measurements.

Clearly a stable RE is essential for OCP measurements, however the molten chloride salt environment makes this a challenging proposition. The stability of REs has been demonstrated to be both time and temperature dependent, with mullite membranes requiring 15 h to settle into an equilibrium at 650 °C.⁸³ The most common RE in molten chloride salts is the Ag/Ag⁺ system in the same matrix salt as the bulk solution. This system has been shown to drift at rates of 0.05 to 0.5 mV h⁻¹ depending on AgCl concentration and moisture contamination.^{84–86} The drift is in part due to deposition and dissolution of silver due to thermal gradients.^{84,87,88} Common membrane materials include mullite, alumina, quartz, and borosilicate. Material compatibility with the specific molten chlorides needs to be considered when selecting a membrane. For example, U(IV) reacts with alumina.⁵⁹

An additional challenge in implementing OCP in molten chlorides is the lack of established and consistent standard states for calculating E^0 and/or $E^{0'}$ (i.e., apparent standard or formal potential), where $E^{0'}$ combines E^0 and the activity coefficient dependency from the Nernst equation. Both Bagri and Simpson⁸⁹ and Hoover et al.⁹⁰ have observed a strong dependency of $E^{0'}$ or activity coefficients on the selection of reference for the Gibbs free energy of formation. This dependency can affect the value of the activity coefficients or concentrations by as much as three orders of magnitude.⁸⁹ Therefore, when utilizing OCP measurement to predict concentrations, attention needs to be given to the standard states and methodology used to determine E^0 or $E^{0'}$.

Concentration is predicted by 30 for oxidized or reduced species by fixing the activity of either the reduced or oxidized species. Most authors achieve this by use of an electrode surface composed of the analyte of choice, thus making the reduced activity 1. Another novel approach for fixing the activity is surrounding the electrode with yttria stabilized zirconium (YSZ) which traps a constant concentration of O²⁻ ions around the RE.⁹¹

Other Methods and Considerations

There are many other electroanalytical methods (e.g., electrochemical impedance spectroscopy (EIS), differential pulse voltammetry, and rotating electrode techniques) but these additional methods are not presented here because little to no studies using them to measure concentrations in molten chloride salts are available in the open literature.

When performing concentration measurements in molten chloride salts, a variety of complications arise. Several topics are briefly presented in this section that shed light on these complications and potential methods to mitigate their effects.

Electrode surface area measurements.—Surface area measurement is a unique challenge to molten salts. Because molten salt electrochemistry takes place in an opaque furnace, immersion depth cannot be visually confirmed. Furthermore, the specific absorption of any species in molten salts on metals is not well-quantified, eliminating the ability to electrochemically measure the surface area. Three general approaches have been taken in the literature for measuring the surface area: physical measurement, differential height and fixed area.^{92–95} The physical measurement method uses observed salt lengths adhering to the WE and known dimensions of the WE (i.e., diameter) to determine the WE surface area. It is important to account for the effects of surface tension when using

this method.⁹² This is best done by immersing the WE into the salt and allowing enough time for the WE to be wetted by the salt and equilibrate thermally. Simply dipping, then immediately removing the electrode can introduce significant errors (~20%).⁹² The differential height method measures the current at various WE immersion depths or with an array of WEs of different lengths. The change in current with the change in surface area (i.e., depth of WE) is then used with electrochemical relations.^{94,95} The fixed area method restricts the electroactive area of the WE to known amount by sealing an insulator to the WE.⁹³

Radial diffusion.—Radial diffusion is common in molten salt electroanalytical measurements due to the use of wires and rods, as cylindrical electrodes. The effects of radial diffusion are similar to natural convection, resulting in currents higher than predicted in models based on semi-infinite linear diffusion. A simple diagnostic can be used to gauge the significance of radial diffusion based at certain time scales. Error from approximating semi-infinite linear diffusion at a cylindrical electrode is under 5% if:

$$\frac{D_i \tau}{r^2} \leq 3 \times 10^{-3} \quad [31]$$

where τ is the time passed since the potential step ($\tau = \frac{RT}{nF\nu}$ for potential sweep method, with ν referring to the scan rate).^{39,42,46}

Migration and convection.—Mass transfer in a fluid, as described by the Nernst-Planck Eq. 32, predicts contributions from diffusion, migration, and convection to the current (i.e., molar flux) in electrochemical experiments.³⁹

$$J_i = -D_i \nabla C_i - \frac{z_i F}{RT} D_i C_i \nabla \phi + C_i v \quad [32]$$

In 32, J_i is the flux of species i , z_i is the charge of the ion, $\nabla \phi$ is the potential gradient, and v is the velocity profile. Supporting electrolyte is typically used to decrease solution resistance and the effect of migration on the analyte. In the presence of an electric field, ions in solution migrate toward the electrode of their opposite charge. When sufficient supporting electrolyte is present, only a small fraction of the migration current is carried by the analyte and the assumption of semi-infinite linear diffusion introduces little error. When the ratio of supporting electrolyte to analyte concentration decreases below 30:1, for $n = \pm 1$, then the share of migration current carried by the analyte is no longer negligible and the observed current signals depart from those predicted under the assumption of semi-infinite linear diffusion.⁵⁴ A general recommended ratio of 100:1 has been given to ensure negligible migration current, but the experimentalist will need to take into consideration their specific conditions, such as ion charge, diffusion coefficients, and temperature.⁵⁴ Since the entire melted solution consists of electrolyte, as the analyte concentration increases, the concentration of the supporting electrolyte decreases. This creates an upper limit for analyte concentration, above which the relations derived under semi-infinite linear diffusion cannot be applied to predict the concentration.

Natural convection is also prevalent in high temperature molten salts. Electrodes typically extend from the molten salt within the furnace out to the ambient atmosphere. These electrodes experience a difference in temperature anywhere from 400 °C–900 °C. Inevitably, thermal gradients are introduced, particularly in the vicinity of the electrodes. Furthermore, at higher concentrations, natural convection can be induced by significant concentration gradients from the bulk to surface of the WE creating density differences in the solution which generate natural convection.^{96,97} The presence of natural convection causes the measured signal to be greater in magnitude than the values predicted from the relations derived based on diffusion-control (e.g., Cottrell, Randels-Ševčík, Berzins-Delahaý). This is manifested in CV measurements by peak current magnitude departing from the linear trend with $\nu^{1/2}$ at low

scan rates (typically $\leq 50 \text{ mV s}^{-1}$). In extreme cases, natural convection will prevent the formation of a peak in CV and take on the character of a rotating electrode measurement where the current plateaus. However, even if a peak is formed, natural convection may still be augmenting the height of the peak.

Uncompensated resistance.—Uncompensated resistance has been discussed for some methods as an important consideration. In molten salts, the resistance is typically small ($<1 \Omega$), but difficulties in applying microelectrodes in high-temperature molten salts^{98–101} has made the use of macroelectrodes common, resulting in high currents which can create significant ohmic losses. Furthermore, high concentrations are also commonly encountered in molten salts which also lead to higher currents and ohmic losses. In CA, ohmic drop can result in delayed achievement of the diffusion controlled current due to the sharp rise in current following a potential step creating significant ohmic potential drop. In CV, it skews the scan rate in the vicinity of the peak due to the increase in current. In NPV, it stretches the potential-current profile and could possibly affect the diffusional current at short pulse times. In SWV, it can profoundly affect the width, height and shape of the peak.^{72,102} Post-measurement corrections can correct for some of the effects of uncompensated resistance, but where the uncompensated resistance affects vital measurement parameters, like scan rate in CV, mitigation of resistance effects is necessary to maintain the integrity of potential waveform. Most modern potentiostats have the capability to actively compensate for ohmic potential losses. In some cases, 100% compensation is possible,⁵² but often it is required to slightly (80%–90%) undercompensate. Other mitigation techniques include the use of simulation for post-experimental correction or iterative correction to modify the applied waveform.^{103,50}

Diffusion coefficients.—Literature values for diffusion coefficients vary significantly across studies, and even show remarkable variance within a single system depending upon the method employed.¹⁰⁴ These discrepancies are likely due to experimental errors and the misapplication of mathematical models. The methodology for accurate measurement of diffusion coefficients, beyond what it offered by the supplied mathematical models is not treated here. However, the procurement of highly accurate diffusion coefficients in a variety of conditions is essential for accurate measurement of concentration.

Multiple electroactive species.—Most practical applications of electrochemistry to measure concentrations in molten salts will deal with the particularly challenging task of accurately measuring concentration in a system with multiple electroactive species. A variety of studies have been conducted in systems with multiple electroactive species.^{59,60,94,98,105–117} These studies typically find that in deposition reactions the accuracy of concentration measurement is diminished when reduction peaks overlap, and even when separated, the second deposition reaction is affected by the first. Standard reduction potentials indicate that corrosion of typical structural metals will impact the accuracy of the vital measurements for U and Pu in electrorefiners.¹¹⁵ Theoretically, techniques such as SWV, NPV and CA are better suited for multicomponent concentration measurements, while OCP and CV are particularly susceptible to error. A variety of data analysis techniques have been attempted in reducing error from CV measurements including semi-differentiation, tail subtraction and multivariate analysis.^{94,107,111,112,117}

Multivariate analysis.—Multivariate analysis has been treated in depth previously.¹¹⁸ An extremely basic explanation is that a model is fed training data from a system, a number of variables are chosen that are fit with this training data, and the model with fitted variables is then applied to new data. This technique is relatively new and unexplored in literature concerning concentration measurements in molten salts. While this technique shows promise and has been

shown to increase the accuracy of complicated systems, useful application will require consistent updating of the training data set due to evolving conditions in the process.

Additional sources of error.—Additional sources of error may be contributed from electromagnetic noise, mechanical vibration, non-representative salt sampling, chemical analysis, and inherit sensitivity in mathematical expressions. Some suggestions include shielding signal wires to reduce electromagnetic noise; mechanically isolating vibration sensitive equipment; considering the non-homogeneity of a cooled salt and the possibility of selective adsorption between the crucible, electrodes and salt; developing expertise in methods such as ICP-MS; utilizing the standard addition method in ICP-MS and similar chemical analysis to minimize error from matrix effects^{119,120}; and bearing in mind that not all mathematical models are created equally. For example, OCP measurements are sensitive due to the natural logarithm included and the transition time in CP theory is ill-defined.

Methodology

Data was extracted from the literature to compare the practically achievable accuracy and precision of different electrochemical techniques. When the data from literature was not numerically presented in tables, a web-based app, WebPlotDigitizer,¹²¹ was used to extract data from figures. Great care was taken to be as accurate in the extraction method as possible, however some error was introduced ($< 1\%$ error).

To display the data in a concise, readable, and usable manner, only data that was able to be found or converted accurately to wt% is used in the comparison. Those interested in usable data from all the studies that were considered can consult the following list.^{55,59,60,79,90–94,105–112,114–117,122–133} In an effort to present the comparative effectiveness of each technique, criteria were applied to reviewed experiments when analyzing them. Only information presented clearly in the literature was able to be applied. For instance, if the area of the electrode is reported but there is no explanation of the method for measurement, this review could not consider the surface area of the WE to be accurately measured.

Accurate WE area.—For all non-zero current techniques, high-quality area measurements use the fixed surface area technique or a variation of a differential height technique and low-quality measurements use a physical measurement of adhering salt technique. Descriptions of these techniques are given above. For deposition reactions, the electrode surface must be renewed between measurements in order to have repeatable data.^{60,94,116} This renewal is typically achieved by holding an anodic potential for a certain period of time. Inconsistent data may indicate that electrode surfaces and the surrounding electrolyte have not been sufficiently renewed.

Linear diffusion approximation verification.—High-quality measurements maintain parameters in 31 that keep error from the linear approximation under 5%. For CA, NPV, and CP the parameter τ refers to the time since the current or potential was stepped. For CV, τ is dependent on temperature, the number of electrons transferred in the given reaction, and the scan rate. Higher temperatures, shorter measurement times, and larger radii for cylindrical electrodes tend to reduce the error associated with this approximation. A calculated concentration larger than expected may indicate that this approximation did not hold.

Negligible migration and convection.—High-quality measurements mitigate migration and convection by maintaining an electrolyte to analyte ratio of 30:1 and by minimizing deposition time. While this criterion is important, it is neglected in our study because data is evaluated within the context of concentration ranges. Furthermore, the ability to quantify the relative effect of migration and convection on measured current is a complex calculation

involving valance state, diffusion coefficient, cell geometry and concentration. In most cases, computational simulation utilizing 32 is required to quantify the influence of migration. Typically, sufficient data is not presented in published studies to perform these calculations or simulations. If the measured current is higher than expected, this may be a sign of migration or convection.

Valid method parameters and application.—High-quality studies that use techniques such as CA, NPV, and SWV must be applied with parameters such as τ , t_p , t_i , ΔE_s , and ΔE that are properly tuned. These parameters must lie within the specified ranges to be applied to mathematical models. High-quality CV studies compare theoretical E vs I graphs with experimental data to verify that the correct model is applied, medium-quality studies check the linearity of $\nu^{1/2}$ vs I_p and the independence of E_p from ν , and low-quality studies only check the linearity of $\nu^{1/2}$ vs I_p graphs. Studies that apply techniques other than CV fulfill this criterion by applying models only if the solubility of reactants and products and reversibility match that of the model assumptions. In CA, this would involve verifying the independence of the temporal current response with potential and the linearity of I vs $t^{-1/2}$. In SWV, this would involve verifying appropriate frequencies, step potentials and pulse potentials (as discussed previously) and the independence of pulse width from frequency. Measurements which are not reasonably predicted by models indicate that either the measurement parameters or the application of the model may introduce some error to the concentration prediction. In some cases, the measurement parameters can be tuned to the regions where the data is in good agreement with the model to increase the accuracy of predicted concentrations.

IR compensation.—High-quality voltametric sweep measurements compensate for the IR effects on the applied waveform. Low-quality sweep voltametric measurements neglect to compensate for IR. IR may express itself in potential sweep measurements by a horizontal stretching of peaks. The value of the diffusion controlled current in NPV and CA is not heavily influenced by IR drop if the sample time is sufficiently long, but the drop may be significant depending on the application and the concentration may be over-estimated. OCP is exempt from this requirement because the net current is zero. IR compensation is not as vital for CP because the current is constant. This results in a constant IR shift which should not affect the transition time because potential at the beginning and the end of transition period is shifted by the same amount.

Relative error.—For data sets containing predicted concentration vs true concentration measured by inductively coupled plasma mass spectroscopy (ICP-MS) or a comparable technique, relative error is simply calculated for each data point according to Eq. 33:

$$\text{Relative Error} = \frac{|x_m - x_p|}{x_p} * 100\% \quad [33]$$

where x_m is known, or measured, concentration and x_p is the concentration predicted according to the given electrochemical

technique. After a relative error is calculated for each point, an average relative error and the three times the sample standard deviation ($3s$) is calculated. s is used instead of the population standard deviation (σ) is used because the gathered data represents a sample of the population, not the population itself.

For data sets containing an independent component (current, normalized current, etc.) vs known concentration, one data point is removed from the rest and designated the test data (x_t, y_t), where x_t is the known concentration. Remaining points are designated as calibration data. A prediction equation is fitted to the calibration data in a form consistent with theory (usually linear). The independent component (peak current, equilibrium potential, etc.) of the test data (y_t) is plugged into the prediction equation which outputs a predicted value of the concentration (x_p). The relative error is then computed according to Eq. 34.

$$\text{Relative Error} = \frac{|x_t - x_p|}{x_p} * 100\% \quad [34]$$

If CA or NPV techniques were used, a separate prediction equation is used in addition to the linear fit which theoretically accounts for migration,⁹³

$$I = \frac{aC}{1 - bC} \quad [35]$$

where a and b are arbitrary constants. Once the parameters are optimized according to the calibration data, the equation is rearranged for the known concentration (C) in terms of current (I), as follows:

$$C = \frac{I}{a + bI} \quad [36]$$

The optimized parameters are inserted for a and b and the independent component of the test data (y_t) was inserted for current (I). A prediction value for concentration (x_p) is subsequently found and inserted into Eq. 34 to find the relative error. Once again, after all data points have been treated as test data, the relative errors are averaged and a $3s$ window is calculated.

Data was also classified as low concentration ($C_i^* < 2 \text{ wt}\%$), medium concentration ($2 \text{ wt}\% < C_i^* < 5 \text{ wt}\%$), high concentration measurements ($C_i^* > 5 \text{ wt}\%$), as well as single or multiple component systems. Relative errors were treated as previously explained with the following exception: if the data spanned a wide concentration range, only values within the appropriate concentration class were considered as test data.

Results

The following sections outline exceptional research that has been conducted in a molten chloride salt medium for each electrochemical technique. This includes a list of all recent studies, to the best of our knowledge, that made use of this technique as well as a brief overview of some of the best performing studies (accuracy under 4%) in each technique. Accuracy is reported as an average relative

Table III. High accuracy CA results.

Method	Study	Concentration Range	Number of Analytes	Analyte	Average Relative Error	Precision ($\pm 3s$)
CA	110	Low	Multiple	Mg(II)	1.64%	2.86%
CA	110	Low	Multiple	La(III)	1.88%	3.23%
CA	110	Medium	Multiple	La(III)	1.85%	2.20%
RCA ^{a)} Anodic Charge	124	High	Single	Nd(III)	1.05%	1.73%
RCA Anodic Charge	124	High	Single	Nd(III)	3.43%	1.99%
RCA Current	124	High	Single	Nd(III)	3.67%	3.47%

a) Analysis includes the use of a non-linear calibration curve model developed by Rappleye et al.⁹³

error and precision is reported as ± 3 s of the relative errors, as explained above.

Chronoamperometry.—This potentiometric step method has been applied to La(III),¹¹⁰ Mg(II),^{107,110} Mn(II),¹²⁶ Nd(III),¹²⁴ and U(III)¹⁰⁷ in LiCl-KCl. Best performing results can be found in Table III.

A 2016 study by Wang et al. measured Mg(II) and La(III) in LiCl-KCl.¹¹⁰ The remarkable results may have been even further improved by a stricter adherence to shorter sample times that would better justify the linear diffusion approximation.

Another notable study is the 2014 work done by Kim et al. Using repeated chronoamperometry (RCA), they measured Nd(III) in LiCl-KCl via anodic and cathodic charge, as well as the current.¹²⁴ Unfortunately, this study did not include any information about WE surface area.

Cyclic voltammetry.—CV has been applied to Gd(III),^{59,112,117} La(III),¹¹⁰ Mg(II),^{107,117} Mn(II),¹²⁶ Nd(III),¹²⁴ Pu(III),¹¹⁶ Sm(III),^{129,130} U(III)^{55,59,90,92–94,107,116,129} in LiCl-KCl, and Mg(OH)⁺ in MgCl₂-KCl-NaCl^{127,134} and various MgCl₂-NaCl mixtures.¹³⁵ It has also been used for oxide ion measurements in CaCl₂.^{131–133} Best performing results can be found in Table IV. Semi-differential analysis of CV is not evaluated in this study due to its limited application.

In 2014, Kim et al. investigated the possibility of using peak area, rather than peak height in the prediction of density with remarkable success.¹²⁴ The method of area determination and *IR* compensation were not addressed. Additionally, the scan rate used in this study did not satisfy the linear-diffusion approximation. Regardless, the impressive accuracy even at high concentration levels is remarkable.

A 2015 study conducted by Tylka et al.¹¹⁶ measured the concentrations of U(III) and Pu(III) in LiCl-KCl with remarkable accuracy. This study used a differential height method to determine WE area, an anodic electrode cleaning procedure between measurements, scan rates that maintained the validity of the linear-diffusion approximation, and currents that resulted in negligible *IR* drop. Semi-differentiation improved the accuracy of the predicted Pu concentration, which was not considered in Table IV.

A 2019 study on Sm(III) in LiCl-KCl conducted by Andrews and Phongikaroon was very accurate, meeting requirements for the linear-diffusion approximation and compensating for *IR* drop. This study may have been even more accurate had a more advanced method of area measurement been used.¹²⁹

Rappleye et al. studied U(III) in LiCl-KCl in 2016. Remarkable accuracy was achieved through use of an electrode with fixed area and scan rates which justified the linear-diffusion approximation, despite the lack of *IR* compensation.⁹²

Hoyt et al. studied the effects of radial diffusion and *IR* drop for U(III) in LiCl-KCl.⁵⁵ Using a correction factor for these two effects, very accurate predictions of concentration were possible. This study used a differential height method to measure WE area and corrected for *IR* drop *post-facto*.

Normal pulse voltammetry.—NPV has been used in studying Gd(III),⁵⁹ La(III),¹¹⁰ Mg(II),^{60,107,108,110} Pu(III),^{109,115} and U(III)^{59,60,92,93,107–109,115} in LiCl-KCl. Best performing results can be found in Table V.

Zhang et al. studied U(III) in LiCl-KCl-MgCl₂ with great success.⁶⁰ The differential height method was utilized to estimate the surface area of the WE, the linear-diffusion approximation was justified, and a model was developed which accounts for both migration and diffusion.^{60,93} This model, while based on theory still requires further validation. However, when applied to the analyzed CA and NPV data the migration model generally improved prediction for high concentration measurements (see Fig. 7).

Rappleye et al. used their glass fused electrode to great affect with NPV. Their study also included a pulse time that maintained the linear-diffusion approximation.⁹³

Another study conducted by Zhang et al. examined Mg(II) in LiCl-KCl-UCl₃. This study satisfied the linear-diffusion approximation and used a differential height method to approximate WE surface area.¹⁰⁸

Wang et al. studied Mg(II) in LiCl-KCl-LaCl₃ and La(III) in LiCl-KCl-MgCl₂. The differential height method was used to predict WE surface area and the linear-diffusion approximation was maintained for the Mg(II) measurements, but may or may not have been justified in the La(III) measurements, depending on the diffusion coefficient of La(III).¹¹⁰

Rappleye et al., mentioned previously, also studies NPV.⁹² However, unlike CV, the compensation of *IR* drop is less essential in non-potential-sweep methods to preserve the signal correlation to concentration if a sufficiently long pulse time is implemented. Unfortunately, the pulse time was not presented in this study.

Yet another study from Zhang et al. performed remarkably well with NPV. This study investigated U(III) in LiCl-KCl, used the differential height method and maintained the linear-diffusion approximation.⁵⁹

Square wave voltammetry.—SWV has been used to study Gd(III),¹²³ La(III),¹²³ and Pu(III)¹¹⁵; and O²⁻ in NaCl-KCl¹²⁸ and LiCl.¹²² Best performing results can be found in Table VI.

In an interesting study performed by Paek et al. the ability of SWV to accurately measure the combined concentration of Gd(III) and La(III) in LiCl-KCl was demonstrated.¹²³ This measurement was not accompanied by any theoretical explanation. Indeed, the theory for deposition SWV offers no explanation for this result.⁷² The study performed by Paek et al. made no mention of information needed to discern the area measurement method, the validity of the linear-diffusion approximation or *IR* drop effects.

Song et al. measured O²⁻ in NaCl-KCl. This study does not clearly state the method used to measure the WE, but did include a correction for meniscus height. It also did not provide information needed to understand the state of the linear-diffusion approximation or *IR* drop.¹²⁸

Table IV. High accuracy CV results.

Method	Study	Concentration Range	Number of Analytes	Analyte	Average Relative Error	Precision (± 3 s)
CV Anodic Charge	124	High	Single	Nd(III)	1.09%	1.36%
CV	124	High	Single	Nd(III)	1.65%	4.58%
CV Cathodic Charge	124	High	Single	Nd(III)	2.12%	4.12%
CV	116	Low	Single	U(III)	2.21%	5.76%
CV	129	High	Single	Sm(III)	2.54%	0.81%
CV	92	Low-Medium	Single	U(III)	2.97%	^{b)}
CV ^{c)}	55	High	Single	U(III)	3.13%	7.24%
CV	116	Low	Single	Pu(III)	3.76%	^{a)}

a) In the specified range, there was only one data point, not allowing for precision to be measured. b) Relative error was reported in the study with no accompanying precision. c) This study made use of a correction for radial diffusion and *IR* drop.

Table V. High accuracy NPV results.

Method	Study	Concentration Range	Number of Analytes	Analyte	Average Relative Error	Precision (± 3 s)
NPV	60	Medium	Multiple	U(III)	0.02%	0.01%
NPV	93	Medium	Single	U(III)	0.31%	0.73%
NPV ^{a)}	93	Medium	Single	U(III)	0.64%	0.72%
NPV	108	Low	Multiple	Mg(II)	1.21%	5.10%
NPV	110	Low	Multiple	Mg(II)	1.31%	2.74%
NPV	92	Low-High	Single	U(III)	1.67%	^{b)}
NPV	93	Low	Single	U(III)	2.26%	4.96%
NPV	60	Low	Multiple	U(III)	2.30%	6.37%
NPV	110	Medium	Multiple	La(III)	2.54%	1.88%
NPV	110	Low	Multiple	La(III)	2.88%	3.83%
NPV	92	Low-Medium	Single	U(III)	2.97%	^{b)}
NPV ^{a)}	59	High	Single	U(III)	3.45%	8.42%
NPV ^{a)}	59	Medium	Single	U(III)	3.76%	8.09%
NPV	59	High	Single	U(III)	3.89%	10.06%
NPV	60	High	Multiple	U(III)	3.95%	11.35%

a) Analysis includes the use of a non-linear calibration curve model developed by Rappleye et al.⁹³ b) Relative error was reported in the study with no accompanying precision.

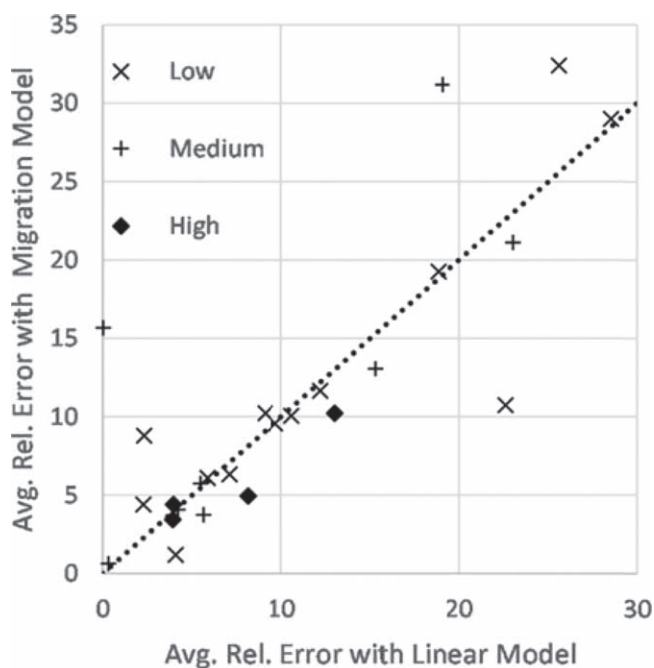


Figure 7. Comparative accuracy of the linear model and the migration model applied to NPV and CA data from literature.

Table VI. High accuracy SWV results.

Method	Study	Concentration Range	Number of Electroactive Species	Analyte	Average Relative Error	Precision (± 3 s)
SWV	123	Low	Multiple	Gd(III) & La(III)	2.09%	3.76%
SWV	128	Low	Single	O ²⁻	3.91%	11.87%

Chronopotentiometry.—CP was used to study Cu(I), Ag(I), Bi(III), Cd(II),⁷⁹ and Mn(II)¹²⁶ in LiCl-KCl. Best performing results can be found in Table VII.

The Laitinen and Ferguson paper from 1957 explored the use of CP in measuring concentration with incredible accuracy, although the metal ion concentrations were quite low. Electrode area was fixed by sealed glass, a sufficiently high current step was chosen so that the linear-diffusion approximation was justified and τ was

calculated by measuring from the departure of the response curve from the tangent line of the inflection point prior to the plateau and the beginning of the response curve's next plateau.⁷⁹

Horvath et al. used a differential height method to approximate WE surface area and used a current step appropriate to satisfy the linear-diffusion approximation.¹²⁶

Open-circuit potentiometry.—OCP was used to study O²⁻ in LiCl,⁹¹ as well as Mg(II)¹⁰⁷ and U(III)^{107,125} in LiCl-KCl. There is no accompanying table for this technique because only one measurement achieved the required accuracy.

Cao et al. developed several REs for use in molten LiCl. Among these REs, was one with a yttria stabilized zirconia membrane. This RE trapped O²⁻ ions around the electrode allowing for very accurate readings.⁹¹ This study measured a low concentration of O²⁻ ions with an average relative error of 3.65% and precision (± 3 s) of 4.70%.

Rappleye et al.¹⁰⁷ did not achieve an accuracy under 4% when utilizing OCP in a multiple analyte mixture. They noted that OCP measurements are complicated for multianalyte mixtures by the simultaneous reactions occurring at the WE. A true equilibrium potential measurement for the more active species is not possible when multiple species are present in the salt. The cell current may be set to zero, but the electrochemical reaction of the more active species will not be at equilibrium (i.e., zero current) because the more noble species is still reducing. In their case, they performed OCP measurements in eutectic LiCl-KCl with both U³⁺ and Mg²⁺ ions present. OCP yielded the highest average relative error and

greatest variability in error for predicting the concentration of Mg²⁺ ions. They concluded that the more active ion in a multianalyte mixture will need to be isolated to measure its true equilibrium potential.

Table VII. High accuracy CP results.

Method	Study	Concentration Range	Number of Analytes	Analyte	Average Relative Error	Precision (± 3 s)
CP	79	Low	Single	Cu(I)	0.11%	0.20%
CP	79	Low	Single	Ag(I)	0.24%	0.77%
CP	79	Low	Single	Bi(III)	0.45%	0.83%
CP	79	Low	Single	Cd(II)	2.87%	11.65%
CP	126	Low	Single	Mn(II)	3.45%	8.79%

Discussion

General areas for future improvement include thoroughly reporting experimental information to ensure that experiments are repeatable and comparable, verifying the applicability of theory, and developing additional theoretical models.

Publications need to include more experimental information if they are to be maximally useful to the community. Some papers achieved remarkable levels of accuracy but did not report the method of WE area measurement, the parameters needed to verify the semi-infinite linear diffusion approximation, nor the use of *IR* compensation or correction. Other studies failed to report all the parameter settings for a particular method. For example, frequency is commonly reported in SWV, but step and/or modulation potential are often omitted. Because of this, the reader can make no inferences about what part of their experimental technique resulted in the accurate results. The following information is recommended to be included in published studies to maximize its benefit to the molten salt electrochemistry community: the method of WE area measurement, the application and amount of *IR* compensation, component weights and/or concentrations of each sample, and electrochemical technique parameters. Important electrochemical parameters include, but are not limited to, scan rate for CV, sample time for CA, frequency, step potential, and square wave amplitude for SWV. Most ideally, the experimental data would be compared with predicted values from theoretical models, when possible, to verify applicability.

Verifying the applicability of theoretical models can drive innovation in developing models where the data doesn't agree and improve the quality of reported values such as diffusion coefficients that are calculated from these models. The ideal approach for determining applicability of a model is to compare experimental curves (e.g., *I* vs *E*, *I* vs *t*) to theoretical model curves. This method may not always be practical because of the scope of variables that may be required to plot the theoretical curve; however, the linearity or independence of measure values can easily be verified.

Developing additional theoretical models will naturally follow as systems are encountered that are not well described by current models. One model in particular to be developed and explored is SWV for deposition reactions. The continued availability of computing resources means that future work can make frequent use of numerical methods to construct customized theoretical models. These models will be especially important when studying systems where radial diffusion, migration and convection are significant.

Conclusions

This review presents the theory of frequently used electrochemical techniques with an emphasis on elements relevant to molten chloride salts. The electroanalytical techniques are compared by their accuracy in predicting the concentration of species in molten salts. Theoretical treatment of each technique includes the assumptions that were used in the derivation of established mathematical models and methods for choosing the correct model. Available data was compiled either directly from tables supplied in the literature or extracted from graphs. Each study which supplied data is evaluated with an established rubric. Data was classified by associated electrochemical technique, the number of electroactive species in the melt, and the concentration range. The low concentration range

data sets were under 2 wt%, medium between 2 and 5 wt%, and high above 5 wt%.

Every electroanalytical measurement technique surveyed was able to measure the concentration of metallic species within a 4% relative error. From the analyzed data, OCP, CP, and SWV only achieved this level of accuracy for low concentrations, while CA, CV, and NPV all have achieved this level of accuracy for low, medium, and high concentrations. Surveyed CA and CV data were only able to achieve this high level of accuracy for high concentrations when only a single component was measured. OCP is neither accurate, nor precise, for the more active species in multianalyte mixtures. NPV was able to reach a high level of accuracy with multiple and single analytes at all defined concentration ranges. Precision generally follows the same trends as accuracy.

Acknowledgments

This work was funded by the College of Engineering at Brigham Young University. Data analysis and visualization was aided by Daniel's XL Toolbox add-in for Excel, version 7.3.2, by Daniel Kraus, Würzburg, Germany (www.xltoolbox.net).

ORCID

Tyler Williams  <https://orcid.org/0000-0002-7206-114X>
Devin Rappleye  <https://orcid.org/0000-0002-4008-7193>

References

1. E. Aghion and G. Golub, *Magnesium Technology: Metallurgy, Design Data, Applications*, ed. H. E. Friedrich and B. L. Mordike (Springer, Berlin, Heidelberg)29 (2006).
2. G. Shekhovtsov, V. Shchegolev, V. Devyatkin, A. Tatakin, and I. Zabelin, *Essential Readings in Magnesium Technology*, ed. S. N. Mathaudhu, A. A. Luo, N. R. Neelameggham, E. A. Nyberg, and W. H. Sillekens (Springer, Cham, Switzerland)97 (2016).
3. R. L. Thayer and R. Neelameggham, *JOM*, **53**, 15 (2001).
4. W. A. Averill and D. L. Olson, *Energy*, **3**, 305 (1978).
5. D. R. Sadoway, *JOM*, **50**, 24 (1998).
6. X. Zhang, A. Han, and Y. Yang, *J. Mater. Chem. A*, **8**, 22455 (2020).
7. N. Krishnamurthy and C. K. Gupta, *Miner. Process. Extr. Metall. Rev.*, **22**, 477 (2002).
8. K. S. Mohandas, *Miner. Process. Extr. Metall.*, **122**, 195 (2013).
9. A. M. Abdelkader, K. T. Kilby, A. Cox, and D. J. Fray, *Chem. Rev.*, **113**, 2863 (2013).
10. K. Ono and R. O. Suzuki, *JOM*, **54**, 59 (2002).
11. G. Z. Chen, D. J. Fray, and T. W. Farthing, *Nature*, **407**, 361 (2000).
12. T. Bauer, C. Odenthal, and A. Bonk, *Chem. Ing. Tech.*, **93**, 534 (2021).
13. R. Serrano-López, J. Fradera, and S. Cuesta-López, *Chem. Eng. Process.*, **73**, 87 (2013).
14. W. Ding, A. Bonk, and T. Bauer, *AIP Conf. Proc.*, **2126**, 200014 (2019).
15. W. Ding and T. Bauer, *Engineering*, **7**, 334 (2021).
16. H. Kim et al., *Chem. Rev.*, **113**, 2075 (2013).
17. Z. Mausloff, M. DeHart, and S. Goluoglu, *Nucl. Eng. Des.*, **379**, 111181 (2021).
18. A. T. Cisneros, K. Czerwinski, B. S. El-Dasher, W. M. Kerlin, K. Kramer, J. F. Latkowski, R. C. Petroski, and J. C. Walter, *Molten Nuclear Fuel Salts and Related Systems and Methods* (2015), US20160189813A1 (<https://patents.google.com/patent/US20160189813A1/en>).
19. I. Scott, *Molten Salt Reactors and Thorium Energy*, ed. T. J. Dolan (Woodhead Publishing, Duxford, United Kingdom)21, 571 (2017).
20. National Research Council, *Electrometallurgical Techniques for DOE Spent Fuel Treatment: Final Report* (The National Academy Press, Washington DC) (2000).
21. T. Paget, J. A. McNeese, K. Fife, M. Jackson, and R. Watson, "Molten Salt Chemistry of Plutonium." *Plutonium Handbook* (American Nuclear Society, La Grange Park, IL) 16 (2019).
22. J. P. Ackerman, *Ind. Eng. Chem. Res.*, **30**, 141 (1991).

23. L. J. Mullins, J. A. Leary, A. N. Morgan, and W. J. Maraman, *Ind. Eng. Chem. Proc. Des. Dev.*, **2**, 20 (1963).
24. J. L. Willit, W. E. Miller, and J. E. Battles, *J. Nucl. Mater.*, **195**, 229 (1992).
25. D. Rappleye, J. McNeese, R. Torres, K. Holliday, and J. R. Jeffries, *J. Nucl. Mater.*, **552**, 152968 (2021).
26. K. Otake, H. Kinoshita, T. Kikuchi, and R. O. Suzuki, *Electrochim. Acta*, **100**, 293 (2013).
27. L. Hu, Y. Song, J. Ge, J. Zhu, and S. Jiao, *J. Mater. Chem. A*, **3**, 21211 (2015).
28. W. Ding, A. Bonk, and T. Bauer, *Front. Chem. Sci. Eng.*, **12**, 564 (2018).
29. S. S. Raiman and S. Lee, *J. Nucl. Mater.*, **511**, 523 (2018).
30. M. Paunovic and M. Schlesinger, *Fundamentals of Electrochemical Deposition* (Wiley, Hoboken, New Jersey)55 (2006).
31. M. Paunovic and M. Schlesinger, *Fundamentals of Electrochemical Deposition* (Wiley, Hoboken, New Jersey)77 (2006).
32. E. L. Compere, S. S. Kirslis, E. G. Bohlmann, F. F. Blankenship, and W. R. Grimes, *Fission product behavior in the Molten Salt Reactor Experiment* (Oak Ridge National Laboratory, Oak Ridge, TN) (1975).
33. E. Capelli, O. Beneš, and R. J. M. Konings, *J. Nucl. Mater.*, **501**, 238 (2018).
34. International Atomic Energy Agency, *IAEA Safeguards Glossary: 2001 Edition* (International Atomic Energy Agency, Vienna) (2002).
35. J. B. Coble, S. E. Skutnik, S. N. Gilliam, and M. P. Cooper, *Nucl. Technol.*, **206**, 1803 (2020).
36. G. L. Fredrickson et al., *J. Electrochem. Soc.*, **166**, D645 (2019).
37. K.-H. Lubert and K. Kalcher, *Electroanalysis*, **22**, 1937 (2010).
38. H. A. Laitinen, *Electrochemistry, Past and Present, ACS Symposium Series*. (American Chemical Society, Washington, DC) 390, 417 (1989).
39. A. J. Bard and L. R. Faulkner, *Electrochemical Methods: Fundamentals and Applications* (Wiley, Hoboken, NJ) 2nd ed. (2001).
40. F. G. Cottrell, *Z. Phys. Chem. Stöchiom. Verwandtschaftsl.*, **42**, 385 (1903).
41. D. M. Gillavry and E. K. Rideal, *Recl. Trav. Chim. Pays-Bas*, **56**, 1013 (1937).
42. A. Szabo, D. K. Cope, D. E. Tallman, P. M. Kovach, and R. M. Wightman, *J. Electroanal. Chem. Interfacial Electrochem.*, **217**, 417 (1987).
43. L. Heerman and A. Tarallo, *J. Electroanal. Chem.*, **470**, 70 (1999).
44. J. E. B. Randles, *Trans. Faraday Soc.*, **44**, 327 (1948).
45. A. Ševčík, *Collect. Czech. Chem. Commun.*, **13**, 349 (1948).
46. T. Berzins and P. Delahay, *J. Am. Chem. Soc.*, **75**, 555 (1953).
47. P. Delahay, *J. Am. Chem. Soc.*, **75**, 1190 (1953).
48. H. Matsuda and Y. Ayabe, *Z. Electrochem. Ber. Bunsengesellschaft Phys. Chem.*, **59**, 494 (1955).
49. I. Atek, S. Maye, H. H. Girault, A. M. Affoune, and P. Peljo, *J. Electroanal. Chem.*, **818**, 35 (2018).
50. D. Krulic, N. Fatouros, and D. Liu, *J. Electroanal. Chem.*, **754**, 30 (2015).
51. D. Shen and R. Akolkar, *J. Electrochem. Soc.*, **164**, H5292 (2017).
52. D. Britz, *Electrochim. Acta*, **25**, 1449 (1980).
53. C. Amatore, C. Lefrou, and F. Pflüger, *J. Electroanal. Chem. Interfacial Electrochem.*, **270**, 43 (1989).
54. E. J. F. Dickinson, J. G. Limon-Petersen, N. V. Rees, and R. G. Compton, *J. Phys. Chem. C*, **113**, 11157 (2009).
55. N. C. Hoyt, J. L. Willit, and M. A. Williamson, *J. Electrochem. Soc.*, **164**, H134 (2017).
56. G. C. Barker and A. W. Gardner, *Z. Anal. Chem.*, **173**, 79 (1960).
57. R. T. Carlin and R. A. Osteryoung, *J. Electrochem. Soc.*, **136**, 1249 (1989).
58. J. Lee, Morris and L. R. Faulkner, *Anal. Chem.*, **49**, 489 (1977).
59. C. Zhang, J. Wallace, and M. F. Simpson, *Electrochim. Acta*, **290**, 429 (2018).
60. C. Zhang, D. Rappleye, and M. Simpson, *J. Electrochem. Soc.*, **164**, H5218 (2017).
61. S. Åberg and M. Sharp, *J. Electroanal. Chem.*, **403**, 31 (1996).
62. G. C. Barker and I. L. Jenkins, *Analyst*, **77**, 685 (1952).
63. L. Ramaley and M. S. Krause, *Anal. Chem.*, **41**, 1362 (1969).
64. J. J. O'Dea, J. Osteryoung, and R. A. Osteryoung, *Anal. Chem.*, **53**, 695 (1981).
65. J. J. O'Dea, J. Osteryoung, and R. A. Osteryoung, *J. Phys. Chem.*, **87**, 3911 (1983).
66. O. J. John, W. Marek, O. Janet, and A. Koichi, *Anal. Chem.*, **57**, 954 (1985).
67. D. P. Whelan, J. J. O'Dea, J. Osteryoung, and K. Aoki, *J. Electroanal. Chem. Interfacial Electrochem.*, **202**, 23 (1986).
68. K. Aoki, K. Tokuda, H. Matsuda, and J. Osteryoung, *J. Electroanal. Chem. Interfacial Electrochem.*, **207**, 25 (1986).
69. K. Aoki, K. Maeda, and J. Osteryoung, *J. Electroanal. Chem. Interfacial Electrochem.*, **272**, 17 (1989).
70. K. Aoki, K. Tokuda, H. Matsuda, and J. Osteryoung, *J. Electroanal. Chem. Interfacial Electrochem.*, **207**, 25 (1986).
71. L. Ramaley and M. S. Krause, *Anal. Chem.*, **41**, 1362 (1969).
72. N. Fatouros and D. Krulic, *J. Electroanal. Chem.*, **706**, 76 (2013).
73. J. J. O'Dea, J. Osteryoung, and R. A. Osteryoung, *Anal. Chem.*, **53**, 695 (1981).
74. B. A. Brookes and R. G. Compton, *J. Phys. Chem. B*, **103**, 9020 (1999).
75. M. A. Mann, J. C. Helfrick, and L. A. Bottomley, *Anal. Chem.*, **86**, 8183 (2014).
76. V. Mirceski, L. Stojanov, and B. Ogorevc, *Electrochim. Acta*, **327**, 134997 (2019).
77. V. Mirceski, E. Laborda, D. Guziejewski, and R. G. Compton, *Anal. Chem.*, **85**, 5586 (2013).
78. H. J. S. Sand, *Philos. Mag.*, **1**, 45 (1901).
79. H. A. Laitinen and W. S. Ferguson, *Anal. Chem.*, **29**, 4 (1957).
80. F. J. Smith, L. M. Ferris, and C. T. Thompson, *Liquid-Vapor Equilibria in LiF-BeF₂ and LiF-BeF₂-ThF₄ Systems ORNL-4415*, Oak Ridge National Laboratory (1969).
81. W. Nernst, *Z. Phys. Chem.*, **4U**, 129 (1889).
82. G. N. Lewis, *Proc. Am. Acad. Arts Sci.*, **43**, 259 (1907).
83. S. Yoon, D. Kang, S. Sohn, J. Park, S. Choi, and M. Lee, *J. Nucl. Fuel Cycle Waste Technol.*, **18**, 143 (2020).
84. L. Yang and R. G. Hudson, *J. Electrochem. Soc.*, **106**, 986 (1959).
85. R.-S. Lin, Y.-Q. Wang, H. He, and G.-A. Ye, *J. Nucl. Radiochem.*, **41**, 447 (2019).
86. C. Zhang, *Electrochemical Measurements in Molten Salt Mixtures for Nuclear Applications, PhD Dissertation*, University of Utah, Salt Lake City (2021).
87. A. C. Gruner and W. T. Thompson, *Can. J. Chem.*, **53**, 1084 (1975).
88. O. Shirai, T. Nagai, A. Uehara, and H. Yamana, *J. Alloys and Compd.*, **456**, 498 (2008).
89. P. Bagri and M. F. Simpson, *J. Nucl. Mater.*, **482**, 248 (2016).
90. R. O. Hoover, M. R. Shalry, S. Martin, K. Sridharan, and S. Phongikaroon, *J. Nucl. Mater.*, **452**, 389 (2014).
91. G. Cao, S. Herrmann, S. Li, R. Hoover, J. King, B. Serrano-Rodriguez, and K. Marsden, *Nucl. Technol.*, **206**, 577 (2020).
92. D. Rappleye, D. Horvath, Z. Wang, C. Zhang, and M. F. Simpson, *ECS Trans.*, **75**, 79 (2016).
93. D. Rappleye, K. Teaford, and M. Simpson, *Electrochim. Acta*, **219**, 721 (2016).
94. M. M. Tylka, J. L. Willit, J. Prakash, and M. A. Williamson, *J. Electrochem. Soc.*, **162**, H852 (2015).
95. N. C. Hoyt, M. A. Williamson, and J. L. Willit, *Multi-electrode Sensor for Concentration and Depth Measurements in Molten Salt*, US20190285565A1 (2019), (<https://patents.google.com/patent/US20190285565A1/en>).
96. M. B. Rooney, D. C. Coomber, and A. M. Bond, *Anal. Chem.*, **72**, 3486 (2000).
97. A. M. Bond, D. C. Coomber, S. W. Feldberg, K. B. Oldham, and T. Vu, *Anal. Chem.*, **73**, 352 (2001).
98. D. K. Corrigan, E. O. Blair, J. G. Terry, A. J. Walton, and A. R. Mount, *Anal. Chem.*, **86**, 11342 (2014).
99. E. O. Blair, D. K. Corrigan, J. G. Terry, A. R. Mount, and A. J. Walton, *J. Microelectromech. Syst.*, **24**, 1346 (2015).
100. D. K. Corrigan, J. P. Elliot, E. O. Blair, S. J. Reeves, I. Schmüser, A. J. Walton, and A. R. Mount, *Faraday Discuss.*, **190**, 351 (2016).
101. E. O. Blair, D. K. Corrigan, H. J. Levene, I. Schmüser, J. G. Terry, S. Smith, A. R. Mount, and A. J. Walton, *IEEE Trans. Semicond. Manuf.*, **30**, 192 (2017).
102. D. Krulic and N. Fatouros, *J. Electroanal. Chem.*, **652**, 26 (2011).
103. D. O. Wipf, *Anal. Chem.*, **68**, 1871 (1996).
104. X. Li, Y. Zhang, B. Yue, L. Yan, T. Jiang, and S. Peng, *J. Mol. Liq.*, **297**, 112106 (2020).
105. M. Stika, D. Rappleye, M. F. Simpson, and S. M. Jeong, *AIChE J.*, **62**, 1236 (2016).
106. D. Rappleye and M. F. Simpson, *J. Nucl. Mater.*, **487**, 362 (2017).
107. D. Rappleye, M. L. Newton, C. Zhang, and M. F. Simpson, *J. Nucl. Mater.*, **486**, 369 (2017).
108. C. Zhang, D. Rappleye, and M. F. Simpson, *ECS Trans.*, **75**, 95 (2016).
109. D. Rappleye, S.-M. Jeong, and M. Simpson, *Ann. Nucl. Energy*, **77**, 265 (2015).
110. Z. Wang, D. Rappleye, C. S. Yang, and M. F. Simpson, *J. Electrochem. Soc.*, **163**, H921 (2016).
111. Z. Wang, D. Rappleye, and M. F. Simpson, *Electrochim. Acta*, **191**, 29 (2016).
112. D. Rappleye, S.-M. Jeong, and M. Simpson, *J. Electrochem. Soc.*, **163**, B507 (2016).
113. H. Zhang, S. Choi, C. Zhang, E. Faulkner, N. Alnajjar, P. Okabe, D. C. Horvath, and M. F. Simpson, *J. Nucl. Mater.*, **527**, 151791 (2019).
114. S. Choi, S.-E. Bae, and T.-H. Park, *J. Electrochem. Soc.*, **164**, H5068 (2017).
115. M. Iizuka, T. Inoue, O. Shirai, T. Iwai, and Y. Arai, *J. Nucl. Mater.*, **297**, 43 (2001).
116. M. M. Tylka, J. L. Willit, J. Prakash, and M. A. Williamson, *J. Electrochem. Soc.*, **162**, H625 (2015).
117. H. Andrews and S. Phongikaroon, *Nucl. Technol.*, **207**, 617 (2021).
118. R. B. Keithley, R. Mark Wightman, and M. L. Heien, *TrAC, Trends Anal. Chem.*, **28**, 1127 (2009).
119. M. Bader, *J. Chem. Educ.*, **57**, 703 (1980).
120. P. Abbyad, J. Tromp, J. Lam, and E. Salin, *J. Anal. At. Spectrom.*, **16**, 464 (2001).
121. A. Rohatgi, (2021), <https://automeris.io/WebPlotDigitizer>.
122. E.-Y. Choi, I.-K. Choi, J.-M. Hur, D.-S. Kang, H.-S. Shin, and S. M. Jeong, *Electrochem. Solid-State Lett.*, **15**, E11 (2011).
123. S. Paek, T.-J. Kim, G.-Y. Kim, D.-H. Ahn, S. Kim, and Y. Jung, *Int. J. Electrochem. Sci.*, **9**, 4925 (2014).
124. D.-H. Kim, S.-E. Bae, T.-H. Park, J.-Y. Kim, C.-W. Lee, and K. Song, *Microchem. J.*, **114**, 261 (2014).
125. D. Yoon and S. Phongikaroon, *J. Electrochem. Soc.*, **164**, E217 (2017).
126. D. Horvath, D. Rappleye, P. Bagri, and M. F. Simpson, *J. Nucl. Mater.*, **493**, 189 (2017).
127. W. Ding, A. Bonk, J. Gussone, and T. Bauer, *J. Energy Storage*, **15**, 408 (2018).
128. J. Song, X. Huang, Y. Fan, J. Yi, Y. Shu, and J. He, *J. Electrochem. Soc.*, **165**, E245 (2018).
129. H. Andrews and S. Phongikaroon, *Nucl. Technol.*, **205**, 891 (2019).
130. H. Andrews and S. Phongikaroon, *Nucl. Technol.*, **206**, 651 (2020).
131. C. Zhang, D. Rappleye, A. Nelson, S. Simpson, and M. Simpson, *J. Electrochem. Soc.*, **168**, 097502 (2021).
132. E. Faulkner, M. Monreal, M. Jackson, and M. F. Simpson, *J. Radioanal. Nucl. Chem.*, **326**, 1289 (2020).
133. M. Mohamedi, B. Børresen, G. M. Haarberg, and R. Tunold, *J. Electrochem. Soc.*, **146**, 1472 (1999).
134. W. Ding, A. Bonk, J. Gussone, and T. Bauer, *Energy Procedia*, **135**, 82 (2017).
135. R. A. Skar, *Chemical and Electrochemical Characterisation of Oxide/Hydroxide Impurities in the Electrolyte for Magnesium Production, PhD Dissertation*, Institutt for Kjemi, Norges Teknisk-Naturvitenskapelige Universitet (2001).